ACS APPLIED MATERIALS & INTERFACES

Research Article

www.acsami.org

Amino-Functionalized Multiwalled Carbon Nanotubes Lead to Successful Ring-Opening Polymerization of Poly(ε-caprolactone): Enhanced Interfacial Bonding and Optimized Mechanical Properties

Eleftheria Roumeli,*[,†] Dimitrios G. Papageorgiou,[†,§,∥] Vasilios Tsanaktsis,[‡] Zoe Terzopoulou,[‡] Konstantinos Chrissafis,[†] Apostolos Avgeropoulos,[⊥] and Dimitrios N. Bikiaris*[,‡]

[†]Solid State Physics Department and [‡]Laboratory of Polymer Chemistry and Technology, Department of Chemistry, Aristotle University of Thessaloniki, Thessaloniki 541424, Greece

[§]School of Materials and [∥]National Graphene Institute, The University of Manchester, Manchester M13 9PL, United Kingdom

[⊥]Polymers' Laboratory, Department of Materials Science Engineering, University of Ioannina, 45110 Ioannina, Greece

Supporting Information

ABSTRACT: In this work, the synthesis, structural characteristics, interfacial bonding, and mechanical properties of poly(ε-caprolactone) (PCL) nanocomposites with small amounts (0.5, 1.0, and 2.5 wt %) of amino-functionalized multiwalled carbon nanotubes (*f*-MWCNTs) prepared by ring-opening polymerization (ROP) are reported. This method allows the creation of a covalent-bonding zone on the surface of nanotubes, which leads to efficient debundling and therefore satisfactory dispersion and effective load transfer in the nanocomposites. The high covalent grafting extent combined with the higher crystallinity provide the basis for a significant enhancement of the mechanical properties, which was detected in the composites with up to 1 wt % *f*-MWCNTs. Increasing filler concentration encourages intrinsic aggregation forces, which allow only minor grafting efficiency and poorer dispersion and hence inferior mechanical performance. *f*-MWCNTs also cause a significant improvement on the polymerization reaction of PCL. Indeed, the in situ polymerization kinetics studies reveal a significant decrease in the reaction temperature, by a factor of 30−40 °C, combined with accelerated the reaction kinetics during initiation and propagation and a drastically reduced effective activation energy.

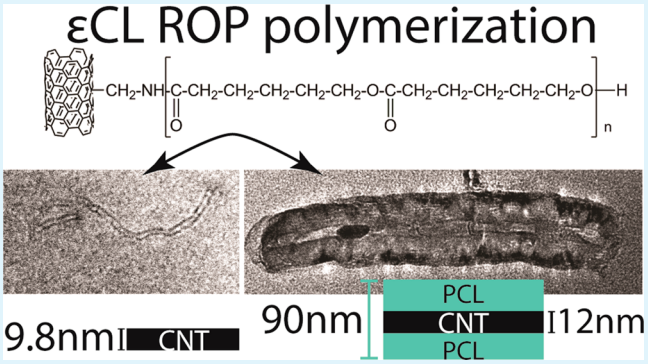

KEYWORDS: *poly(ε-caprolactone), multiwalled carbon nanotubes, nanocomposites, in situ polymerization, mechanical properties*

1. INTRODUCTION

The preparation of polymer nanocomposites has proven to be an efficient way of upgrading the properties of synthetic polymers to a certain point, whereas the final properties of the nanocomposite exceed the ones of conventional composites.[1−3] Several works have reported that even a small amount (ranging from 0.5 to 5 wt %) of an inorganic filler inside a polymeric matrix can improve drastically the performance of the matrix. The most profound effects have been observed for mechanical, thermal, and electrical properties of the final nanocomposites.[4,5]

Additionally, the widespread use of petroleum-based conventional polymers has raised widely spread environmental issues because of their abundant applications. For this reason, several synthetic or naturally synthesized biodegradable polymers such as polyesters have been prepared, studied, and used by both industry and academia, taking into account environmental regulations and guidelines.[6,7] ε-Poly(caprolactone), or PCL, is such an aliphatic semicrystalline polyester that is also biodegradable and biocompatible with many potential applications already reported in literature such as tissue engineering, scaffold preparation, controlled drug release, and others.[8−11] However, the low melting point and the mediocre mechanical performance of PCL generally limit the applications for which it can be used, and therefore, several attempts have been made to improve its properties with the introduction of inorganic fillers.[12−19]

Multiwalled carbon nanotubes (MWCNTs) have been used for reinforcement of polymeric matrixes; starting from the first work of Ajayan et al.,[20] who introduced MWCNTs in an epoxy matrix, a vast amount of reports have been dedicated to the development of polymer/MWCNT nanocomposites.[21−26] The most challenging part of the preparation of a MWCNT-based nanocomposite is the successful dispersion of MWCNTs inside the polymeric matrix because the strong van der Waals

Received: April 29, 2015
Accepted: May 7, 2015
Published: May 7, 2015

DOI: 10.1021/acsami.5b03693
ACS Appl. Mater. Interfaces 2015, 7, 11683−11694

interactions, which are developed between the MWCNTs, force them to curve and form very hard and almost impossible to break bundles.[27,28] For this reason, several preparation strategies, including covalent or noncovalent polymer grafting approaches, have been developed in order to achieve MWCNT debundling and eventually increase the interactions with the polymeric matrix.[29−38] Following the covalent bonding approaches, in this work we utilize ring-opening in situ polymerization (ROP) to produce PCL nanocomposites with amino-functionalized MWCNTs (*f*-MWCNTs) in an effort to create a polymer−nanotube bonding zone that would lead to improved filler dispersion and therefore enhanced mechanical performance.[12,39,40]

Several works have dealt with the grafting of MWCNTs on PCL, but only a few works have reported the preparation of such PCL/MWCNT nanocomposites by in situ polymerization[14,41−43] whereas many others have used alternative preparation methods.[44−47] Moreover, few other authors have reported using ROP to synthesize PCL with *f*-MWCNTs.[48−53] In an recent study, Müller and co-workers reported that the PCL-grafted MWCNTs alter the chain topology of the matrix by forming a transient network, resulting in slower diffusion and relaxation of the cyclic molecules of the matrix.[52] Furthermore, the majority of those studies have shown that MWCNTs play a major role on the polymerization procedure, thereby affecting positively the final structure and properties of the composite materials.

One of the first attempts to prepare PCL nanocomposites with amino-functionalized MWCNTs was reported from Ruelle et al.[54] because of the fact that primary amines have been reported as highly efficient initiators of the ring-opening polymerization of ε-caprolactone (ε-CL).[55] From TEM micrographs, it was found that MWCNTs were successfully grafted with PCL macromolecules. In other studies, amino- or hydroxyl-functionalized MWCNTs have been used to prepare PCL nanocomposites with little or no reference concerning the properties of the prepared nanocomposites.[51,56−59] In a recent study, Kumar et al.[60] reported a 28% enhancement of the tensile strength of melt-mixed PCL/amino-functionalized MWCNT composites. Furthermore, Zhou et al. reported that MWCNTs grafted on PCL cause a faster crystallization rate and a smaller crystal size of the grafting polymers, leading to higher values of T_c and T_m.[59] As it can be realized, the simultaneous application of the ROP procedure, which has been proven to enable exfoliation and homogeneous dispersion of the filler, with the use of functionalized MWCNTs is expected to attribute superior characteristics to the produced nanocomposite samples.

The aim of the present work is to study the effectiveness of *f*-MWCNTs as ROP co-initiators of ε-caprolactone and as reinforcing agents on the formed PCL/MWCNT nanocomposites. Thus, a systematic investigation of the ability of *f*-MWCNTs to create a covalent-bonding zone with the polymer backbone is provided and the detected mechanical properties are well-correlated with the reinforcement of the composites.

2. EXPERIMENTAL SECTION

2.1. Materials. ε-Caprolactone (ε-CL) (purum 99%) and tetrabutyl titanate (TBT) catalyst of analytical grade were purchased from Aldrich Chemical Co. (Stainheim, Germany). *f*-MWCNTs were kindly offered from GLONATECH S.A. (Athens Greece, ONEX-MW 1004 C2). The nanotubes have 5% NH_2 content, average diameter = 15 ± 5 nm, length > 5 μm, and bulk density = 0.2 g cm^3.

2.2. PCL Synthesis and Nanocomposites Preparation. For the synthesis of PCL, ε-CL was dried over CaH_2 and purified by distillation under reduced pressure prior to use. The bulk polymerization of ε-CL was carried out in a 250 mL round-bottomed flask equipped with a mechanical stirrer and a vacuum apparatus. The catalyst TBT was added as a solution in toluene at a final concentration of 1×10^{-4} moles per mole of monomer. The polymerization mixture was degassed and purged with dry argon three times. The polymerization reaction was carried out for 2 h at 180 °C. Unreacted monomer was removed through distillation by applying a high vacuum (~5 Pa) slowly, in order to avoid excessive foaming, over a time period of 15 min. Polymerization was terminated by rapid cooling to room temperature.

For the preparation of PCL/*f*-MWCNT nanocomposites by in situ polymerization, the same technique was used as described above. *f*-MWCNTs together with the proper amount of TBT were added to ε-CL monomer and were sonicated initially for 2 min using a sonicator apparatus and then in a sonic bath for 15 min. For the first polymerization step, all amounts were transferred in a 250 mL round-bottomed flask and heated at 180 °C for 2 h (Scheme 1). Unreacted monomer was removed through distillation by applying a high vacuum (~5 Pa) slowly over a time period of 15 min. Polymerization was again terminated by rapid cooling to room temperature. According to this procedure, nanocomposites containing 0.5, 1, and 2.5 wt % *f*-MWCNTs have been prepared.

Scheme 1. PCL/*f*-MWCNT Nanocomposites Prepared by Ring-Opening Polymerization

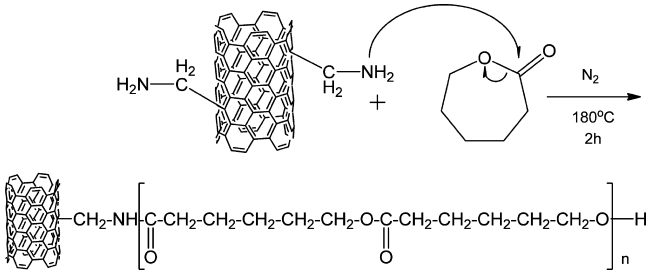

The prepared materials were afterward hot-pressed using an Otto Weber Type PW 30 hydraulic press connected with an Omron E5AX Temperature Controller at a temperature of 75 ± 5 °C, in order to prepare films of different thicknesses therefore appropriate for each type of the following measurements.

2.3. Characterization Methods. Size-exclusion chromatography (SEC) experiments were carried out at 30 °C using a Spectra System PL 1000 pump, a Shodex RI 101 refractive index detector, and a Spectra System UV-1000 detector. Three Mixed-C columns were used (Polymer Laboratories, with pores for efficient separation of molecules varying from 2000 to 4×10^6 g/mol), thermostated in a Lab Alliance column oven at 30 °C. THF, distilled over CaH_2 and sodium, was the carrier solvent at a flow rate of 1 mL/min.

Intrinsic viscosity (η) measurements were performed using an Ubbelohde viscometer at 30 °C in a mixture of phenol/tetrachloroethane 60:40 w/w. The sample was maintained in the solvent at room temperature for some time in order to achieve a complete solution. The solution was then filtered through a disposable membrane filter made from Teflon.

Differential scanning calorimetry (DSC) measurements were carried out in a calibrated Setaram DSC (model 141) in order to monitor in situ polymerization.[61] From each mixture, a 15 ± 1 mg sample was placed in stainless-steel sealed crucibles, whereas an identical empty crucible was used as reference in each measurement. The samples were heated from ambient temperature (25 °C) to 250 °C under a 50 mL/min flow of N_2 with heating rates of 1, 2.5, and 5 °C min^{-1} in order to study the polymerization kinetics. The effective activation energy of

DOI: 10.1021/acsami.5b03693
ACS Appl. Mater. Interfaces 2015, 7, 11683−11694

polymerization was calculated by the isoconversional method of Starink.

Ultrathin film samples of the nanocomposites were prepared through cryomicrotoming at −90 °C with a DIATOME cryo-45° diamond knife by the ultramicrotome Leica EM FC7. Transmission electron microscopy (TEM) images of the thin sections were placed on copper grids and studied using a JEOL HR-JEM 2100 electron transmission microscope operating at 200 kV.

X-ray photoelectron spectroscopy (XPS) spectra were acquired in an Axis Ultra DLD system by KRATOS. A monochromated Al Kα_1 X-ray beam was used as the excitation source. The pass energy was 160 eV for survey scans and 20 eV for high resolution spectra.

Wide angle X-ray diffraction (WAXD) measurements of the samples were performed using a MiniFlex II XRD system from Rigaku Co, with CuKα radiation (λ = 0.154 nm) in the area of 5° < 2θ <60°. Crystallinity calculations of the studied materials were performed by fitting the WAXD profiles with Gaussian−Lorentzian cross-product curves and deriving the ratio of crystallinity over overall fitted peaks area.[62,63]

Calculations of the size of crystalline domains (L) in the main crystallographic directions have been performed using Scherrer's equation[64]

$$L = \frac{0.9\lambda}{B\cos\theta} \quad (1)$$

where B is the full width at half-maximum (fwhm) of the corresponding peak and λ is the wavelength of Cu Kα radiation ($\lambda_{CuK\alpha}$ = 1.5418 nm).

Measurements of tensile mechanical properties of the prepared nanocomposites were performed on an Instron 3344 dynamometer, in accordance with ASTM D638, using a crosshead speed of 50 mm min^{-1}. Dumbbell-shaped tensile test specimens (central portions, 5 × 0.5 mm thick, 22 mm gauge length) were cut in a Wallace cutting press from100 μm thick film, prepared as described before, in an Otto Weber hydraulic press and conditioned at 25 °C and 55−60% relative humidity for 48 h. From stress−strain curves, the values of tensile strength at the yield point and at break, elongation at break, and Young's modulus were determined. The toughness was calculated from the area under the obtained stress−strain curves as described elsewhere.[65] Izod impact tests were performed using a Tinius Olsen apparatus in accordance with ASTM D256 method. In both cases, five samples were measured, and the results were averaged to obtain a mean value.

A Renishaw system 1000 spectrometer coupled to a 633 nm HeNe laser was used to record Raman spectra from PCL and nanocomposite samples. The laser was focused on the samples using a ×50 lens (numerical aperture = 0.60) to a spot size of 2.0 μm, and spectra were recorded using an exposure time of 10.0 s and three accumulations. This exposure time was chosen to minimize the heating effects that can cause shifts in the position of Raman peaks obtained from the carbon-based filler.

3. RESULTS AND DISCUSSION

3.1. Effect of *f*-MWCNTs on Ring-Opening Polymerization of ε-CL. Simulating the polymerization process through DSC experiments provides useful information regarding the kinetics of the reaction and the effects of the filler in the process. In Figure 1a, the heat-flow curves of all the prepared materials collected at a heating rate of 1 K min^{-1} are presented, revealing the significant influence of the incorporation of *f*-MWCNTs in PCL. In Figure 1b,c, the calculated monomer conversion degree (or extent of polymerization, α) is plotted versus temperature and time, respectively, for the same heating rate. A gradual shift (as large as 30−40 °C) of the whole polymerization reaction toward lower temperatures with increasing *f*-MWCNT concentration was evident in every set of experiments. As can be seen in Table 1, the shift depends also on the applied heating rate. This notable shifting for every employed heating rate reveals the significant influence of *f*-MWCNTs on the polymerization reaction of ε-CL. Further-

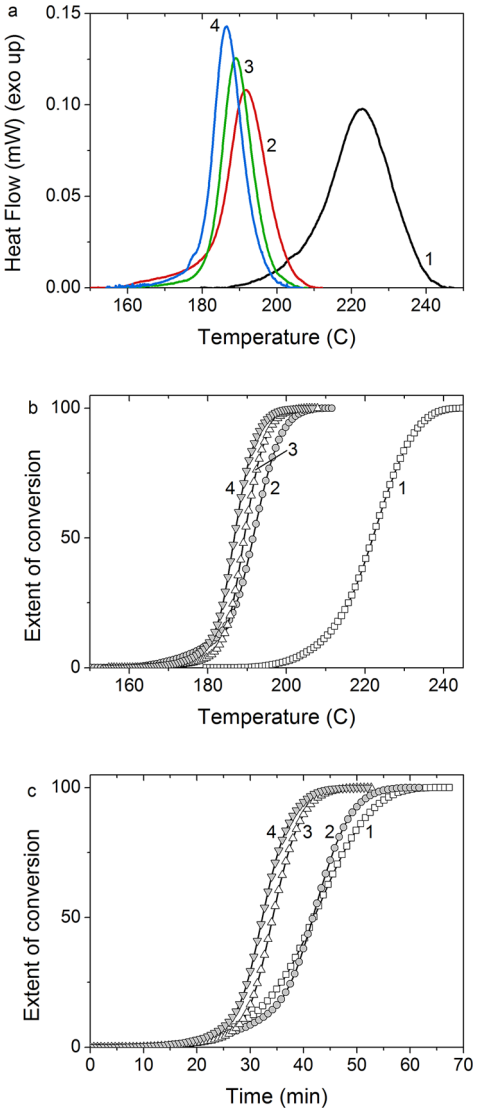

Figure 1. (a) Heat-flow curves of ring-opening polymerization collected at rate = 1 K min^{-1} and the corresponding extent of conversion dependence on (b) temperature and (c) time for: (1) PCL, (2) PCL/0.5 wt % *f*-MWCNTs, (3) PCL/1 wt % *f*-MWCNTs, and (4) PCL/2.5 wt % *f*-MWCNTs.

Table 1. Polymerization Peaks of Neat ε-CL and in the Presence of *f*-MWCNTs at Different Heating Rates

material	rate (K min^{-1})	peak (°C)
PCL	1	221
	2.5	244.5
	5	254.3
PCL/0.5 wt % *f*-MWCNTs	1	191
	2.5	209.9
	5	230.7
PCL/1 wt % *f*-MWCNTs	1	188.8
	2.5	212.4
	5	231.4
PCL/2.5 wt % *f*-MWCNTs	1	184.3
	2.5	200.35
	5	226.9

DOI: 10.1021/acsami.5b03693
ACS Appl. Mater. Interfaces 2015, 7, 11683−11694

more, the total width of the exothermic peaks is also notably lower in the nanocomposites compared to neat PCL, indicating that *f*-MWCNTs not only enable the initiation of the process at lower temperatures but also accelerate the whole reaction. For the nanocomposites with 1 and 2.5 wt % *f*-MWCNTs, this observation can be verified in the monomer conversion versus time curves, shown in Figure 1c. Such an important shift to lower temperatures combined with a faster polymerization reaction will lead to advantages concerning the incorporation of functionalized carbon nanofillers in industrially produced PCL because the decrease in the required polymerization temperature and the lower processing times remain two of the main requirements for inexpensive production in the polymer industry.

To examine the effects of *f*-MWCNTs on the kinetics of polymerization, the obtained exothermic curves were subjected to analysis with the integral isoconversional method of Starink.[66] According to the Starink's method, the extent of conversion (α) corresponding to the normalized monomer conversion degree can be incorporated in the following equation in order to obtain the effective activation energy E_A of polymerization:

$$\ln\left(\frac{\beta}{T_{\alpha,i}^{1.92}}\right) = \text{const.} - 1.0008\left(\frac{E_A}{RT_\alpha}\right) \quad (2)$$

where β is the heating rate and R is the gas constant. The index i is introduced to denote various temperature programs. $T_{\alpha,i}$ is the temperature at which a certain extent of conversion value, α, is reached under the temperature program i. The E_A values are obtained through the slope of the plot of $\ln(\beta/T_{\alpha,i}^{1.92})$ versus $(1/T_\alpha)$.

The calculated effective activation energy values versus the degree of conversion were plotted for all the prepared materials and are presented in Figure 2. It was realized that the energy

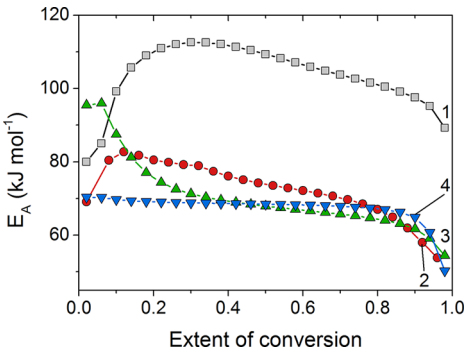

Figure 2. Effective activation energy dependence on extent of polymerization as calculated using Starink's method for (1) PCL, (2) PCL/0.5 wt % *f*-MWCNTs, (3) PCL/1 wt % *f*-MWCNTs ,and (4) PCL/2.5 wt % *f*-MWCNTs.

barrier of polymerization is significantly reduced in the presence of *f*-MWCNTs, an observation which confirms that the filler in fact allows the beginning of polymerization at lower temperatures. Specifically, PCL was found to have an initially increasing activation energy from 80 to 110 kJ mol^{-1} followed by a marginal decrease, which began at approximately 40% of the reaction. This dependence of effective activation energy on the extent of polymerization suggests that this process requires more than one reaction mechanism to be adequately described.[67]

Through the incorporation of 0.5 wt % *f*-MWCNTs, a smaller increase of the activation energy concerning the initial 20% of the reaction was followed by a continuous drop through the completion of the reaction. Therefore, both the absolute effective activation energy and the involved mechanisms seem to have been modified from the incorporation of *f*-MWCNTs in polymerization. For the composite with 1 wt % *f*-MWCNTs, the activation energy decreased from 100 to 70 kJ mol^{-1} for the initial 20% of the reaction and remained almost constant until 90% of the reaction. Then, a further decrease was detected for the final polymerization steps. Thus, increasing *f*-MWCNTs content modifies further the polymerization kinetics of PCL. The material with the highest nanofiller percentage presented an even further modified activation energy trend. In that case, the effective activation energy remained almost constant through most of the reaction and a drop was detected at the final polymerization steps, that is, after 90% of the reaction had been completed. Therefore, from Starink's method, it was proven that the incorporation of *f*-MWCNTs decreases the energy barrier of polymerization and probably interferes with the relative reaction models involved in the specific polymerization.

3.2. Nanocomposite Morphology and Molecular Characteristics. In Figures 3 and 4, characteristic TEM

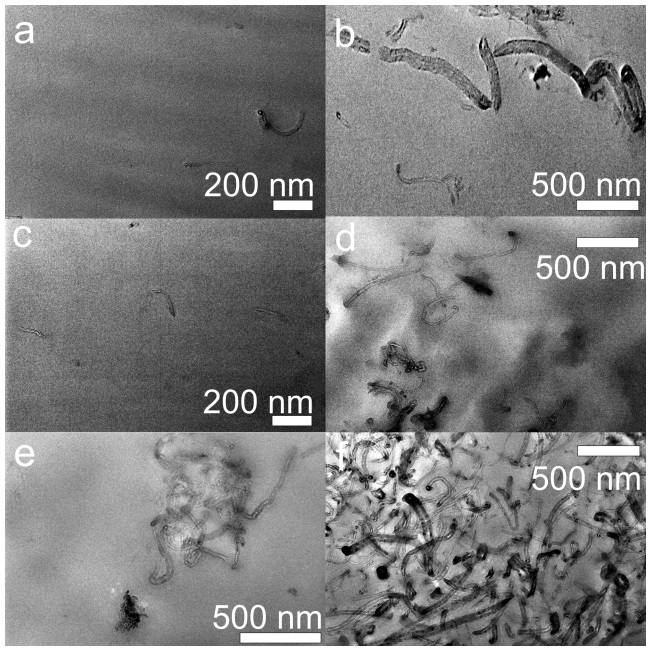

Figure 3. TEM images of (a and b) PCL/0.5 wt % *f*-MWCNTs, (c and d) PCL/1 wt % *f*-MWCNTs, and (e and f) PCL/2.5 wt % *f*-MWCNTs.

images of the prepared nanocomposites are presented. In the composites with 0.5 wt % *f*-MWCNTs (Figures 3a,b and 4a), the nanotubes were found to be adequately dispersed in the PCL matrix, whereas no large aggregates were detected in the observed sections. Through these images, a polymer layer surrounding the nanotube core is detected. Although the nanotubes have an outer diameter of approximately 15 nm, a polymer coating of 1−35 nm was observed (Figures 3b and 4a). Similarly, for the composites with 1 wt % *f*-MWCNTs (Figures 3c,d and 4b), the nanotubes were found to be in a mostly debundled state and dispersed in the polymer matrix. The

DOI: 10.1021/acsami.5b03693
ACS Appl. Mater. Interfaces 2015, 7, 11683−11694

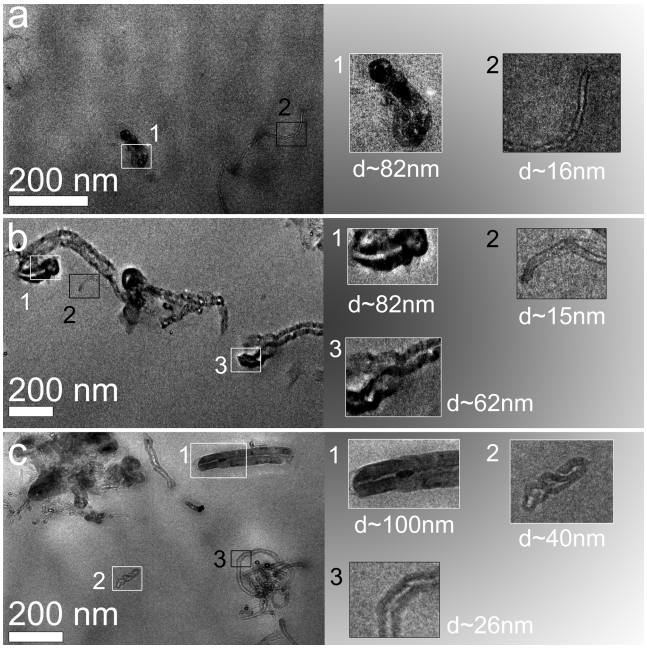

Figure 4. (Left panels) TEM images of (a) PCL/0.5 wt % *f*-MWCNTs, (b) PCL/1 wt % *f*-MWCNTs, and (c) PCL/2.5 wt % *f*-MWCNTs. Detail views of the numbered areas are presented in the right side, depicting the formation of an interface between the nanotubes and the matrix.

polymer coating layer was also observed through the collected images, and its thickness varied from 1 to 35 nm. On the contrary, the observations of the composite with 2.5 wt % *f*-MWCNTs (Figures 3e,f and 4c) revealed large nanotube bundles with sizes reaching 1 μm. However, in that composite, polymer-coated nanotubes were once again detected (Figures 3f and 4c) with thicknesses as high as 85 nm. Therefore, some portion of the nanotubes is coated by a polymer layer even at the highest loading, but excessive bundling cannot be avoided.

Overall from the transmission electron microscopy observations, it was revealed that the followed preparation method successfully debundled the nanotubes for the low filler concentrations, whereas when the *f*-MWCNT amount exceeded 1 wt %, several aggregates were formed. From the TEM images and the provided detailed views, it is clear that PCL creates a surface-coating layer on the *f*-MWCNTs, which can be attributed to the formation of covalent bonds between the *f*-MWCNTs and PCL as discussed in the following sections.[32,58,68] Similar core−shell type structures with a stiff carbon nanotube core and a soft polymer surrounding coating have been reported by many other authors for other polymer matrices as well as for PCL.[51,53,69−72] Evidence indicates that this seems to be the case in the present study as well. These bonds not only lead to exfoliation of the nanotubes in the matrix but also should improve the mechanical performance of the materials because they provide large load-transfer channels.

Measurements of intrinsic viscosity as well as SEC measurements were performed in order to evaluate the effect of the nanotubes on the molecular characteristics of the matrix. Additionally, calculations of the mean radius of gyration based on the viscometry and SEC results were performed.[73,74] The critical relationships between nanofiller diamensions, polymer gyration radius, and the final viscosity have been proposed to be related with filler exfoliation state and dispersion.[1,75−78]

According to Flory's equation,[74] the intrinsic viscosity, average molecular weight per weight (M_w), and Flory's constant (Φ) can be used to determine the mean radius of gyration ($\langle \overline{S^2} \rangle^{(3/2)}$) according to the formula:

$$\langle \overline{S^2} \rangle^{3/2} = \frac{[\eta] M_w}{\Phi} \quad (3)$$

In our calculations, we used Flory's constant value of 2.5×10^{21} (when $[\eta]$ is given in dL/g), and the results are summarized in Table 2. SEC revealed a single peak for PCL that had an

Table 2. Intrinsic Viscosity and Mean Radius of Gyration Values for PCL/*f*-MWCNT Composites

sample	$[\eta]$ (dL/g)	$\langle \overline{S^2} \rangle^{(3/2)}$ (nm)
PCL	1.00	28.5
PCL/0.5 wt % *f*-MWCNTs	1.43	32.1
PCL/1 wt % *f*-MWCNTs	1.28	31.0
PCL/2.5 wt % *f*-MWCNTs	0.86	27.1

average molecular weight per number ($\overline{M_n}$) of 37 365 g mol^{-1} and a polydispersity index ($I = \overline{M_w}/\overline{M_n}$) of 1.55. Therefore, the determined molecular weight of PCL was 57 915 g mol^{-1}.

The measurement and calculation results are summarized in Table 2. It is indicted that low amounts of filler (0.5−1 wt %) cause a notable increase on the viscosity of PCL and an enlargement on the mean gyration radius, which are consistent with the exfoliated and debundled state observed in the corresponding TEM images (Figures 3a−d and 4a,b). Additionally, the differences in the gyration radii between the nanocomposites indicate that the presence of the filler has caused certain changes in the packing of the PCL macromolecular chains at the interface between the polymer and the filler. This conclusion should be reflected on the physicochemical properties of the samples. Increased viscosities correlated with covalent filler−matrix bonding were also reported in previous studies on poly(ethylene terepthtalate)[79] and aliphatic polyesters using silica nanoparticles as additives.[80,81]

However, a previous study in PCL/SiO_2 nanocomposites had highlighted that a possible trapping of the active species of the metal alkoxide ring-opening initiator, caused by a heterogeneous exchange reaction between its functional groups and the nanoparticles' surface silanol groups, can lead to decreased viscosity and molecular weight for the composites with higher nanoparticle concentrations.[82] The detected higher aggregation state was consistent with the decreased viscosity and molecular weight of these materials. Therefore, in the case of *f*-MWCNT composites, the existence of such a reaction could not be supported.

Nevertheless, by increasing further the filler content, an important decrease of the viscosity was observed, reaching values lower than those of the neat polymer. Lower viscosity and decreased mean gyration radius can be supported by the bundled and significantly less dispersed state of the nanotubes in that composite. In this concentration, it seems that because of the formation of aggregates some amino groups have not reacted with ε-CL monomer and remained free causing an aminolytic reaction to the formed macromolecules. Another reason could rely on the barrier effect of *f*-MWCNT aggregates, which hinder the ε-CL monomers reaction with macromolecular end groups therefore leading to lower molecular characteristics than expected.

DOI: 10.1021/acsami.5b03693
ACS Appl. Mater. Interfaces 2015, 7, 11683−11694

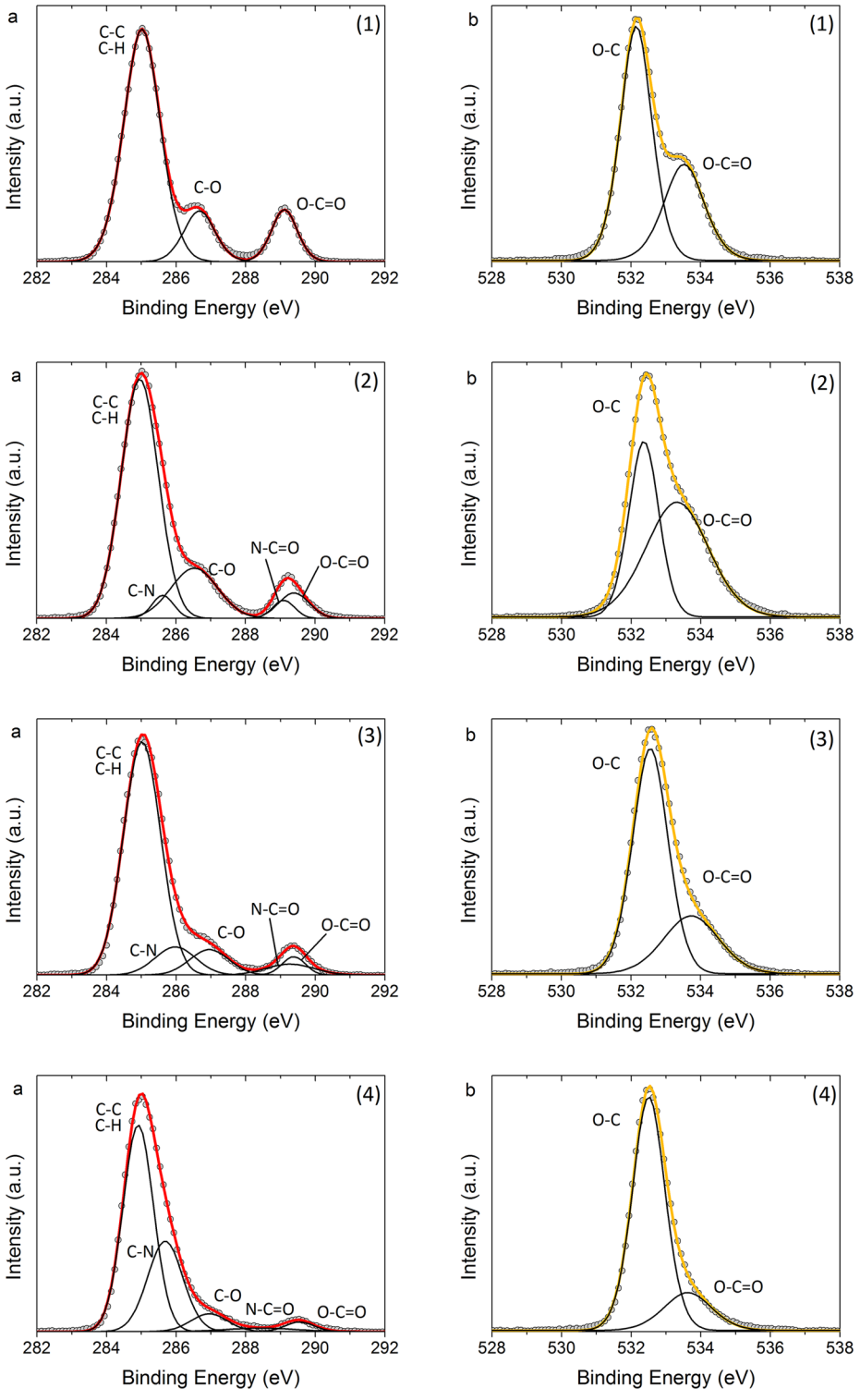

Figure 5. High-resolution XPS spectra of (a) C 1s and (b) O 1s core level and peak deconvolution for all the prepared materials: (1) PCL, (2) PCL/0.5 wt % *f*-MWCNTs, (3) PCL/1 wt % *f*-MWCNTs, and (4) PCL/2.5 wt % *f*-MWCNTs.

3.3. Evaluation of Nanotube Grafting to Polymer Backbone. To evaluate directly the incorporation of *f*-MWCNTs to PCL and the possibility of *f*-MWCNTs to interact with ε-CL forming covalent bonds, XPS measurements were conducted. XPS was used in a previous work to study the grafting procedure of MWCNTs−OH on PCL macromolecules.[58] The obtained wide scans of all the materials, presented in Supporting Information Figure S1, confirmed their carbon and oxygen composition with marginal differences regarding their intensity. The corresponding measurements for *f*-MWCNTs are also presented in Supporting Information Figure S2.

The high-resolution spectra of the C 1s and O 1s core levels were deconvoluted, as presented in Figure 5, to separate the various bonds contributions. The results are grouped in Table 3, and they confirm the successful covalent grafting of the

DOI: 10.1021/acsami.5b03693
ACS Appl. Mater. Interfaces 2015, 7, 11683−11694

Table 3. Bond Positions and Relative Concentrations from Deconvolutions of C 1s and O 1s Core Level XPS Spectra for All the Prepared Materials

	peak positions (eV)					percentages (%)				
	C−C	C−N	C−O	N−C═O	O−C═O	C−C	C−N	C−O	N−C═O	O−C═O
PCL	285.0		286.7		289.1	74.3		13.9		11.9
PCL/0.5 wt % *f*-MWCNTs	285.0	285.6	286.5	289.1	289.4	68.8	3.9	18.2	3.1	6.0
PCL/1 wt % *f*-MWCNTs	285.0	286.0	287.0	289.3	289.4	73.7	9.7	8.5	4.4	3.6
PCL/2.5 wt % *f*-MWCNTs	284.9	285.7	287.0	288.4	289.6	59.2	29.7	6.2	2.3	2.6
	C−C	O−C═O				C−C	O−C═O			
PCL	532.15	533.52				65.4	34.6			
PCL/0.5 wt % *f*-MWCNTs	532.36	533.32				42.2	57.8			
PCL/1 wt % *f*-MWCNTs	532.56	533.73				71.3	28.7			
PCL/2.5 wt % *f*-MWCNTs	532.51	533.62				80.7	19.3			

functionalized nanotubes from the monomer chain through the surface amino groups, proposed in Scheme 1.

In detail, the C 1s and O 1s core level analysis for PCL confirmed the presence of C−C/C−H, C−O, and O−C═O bonds, respectively, through the three characteristic peaks at 285.0, 286.7, and 289.1 eV for C 1s and the two peaks at 532.1 and 533.5 eV for O 1s (Figure 4). Generally, the incorporation of *f*-MWCNTs tends to merge the detected peaks of both C 1s and O 1s. Specifically, increased nanotube content leads to a gradual merge of the collected peaks to one broader collective distribution.

From the deconvolution of the carbon bonding peak, the distinct backbone contributions (C−C/C−H and C−O) along with the new, nanotube-related C−N and N−C═O bonds are revealed as a result of the reaction of surface amino-groups of *f*-MWCNTs with ε-CL. The existence of C−N and N−C═O groups is proof that the amino groups of *f*-MWCNTs can act as initiators for ε-CL, forming covalent bonds with PCL macromolecules. According to the proposed grafting reaction of nanotubes on the ε-caprolactone chains (described in Scheme 1), N−C═O bonds are only formed after covalent bonding of the surface amino groups to the polymer backbone and can therefore serve as a direct indicator of the grafting degree, whereas the C−N bonds, which are present in both the ungrafted and grafted *f*-MWCNTs, can indirectly suggest the grafting degree. It is noteworthy to mention that the relative amount of the N−C and N−C═O bonds is significant concerning the low filler concentrations used in this work. For instance, in the 2.5 wt % *f*-MWCNTs composite, approximately 32% of the overall bond area is associated with the nitrogen−carbon bonds that arise from the bonded and unreacted surface amino groups of the nanotubes collectively.

To evaluate the grafting degree, two indices obtained from the ratios of the peak intensity (G1) and area (G2) of the N−C═O over C−N bonds, respectively, were calculated. As presented in Figure 6, both of the grafting indices yield similar results, according to which the composite with 0.5 wt % *f*-MWCNTs has the highest grafting efficiency (almost 80%). The high degree of covalent bonding between the nanotubes and PCL confirms the previously detected efficient filler exfoliation. The composite with 1 wt % *f*-MWCNTs still maintained a high grafting degree (40−50%), whereas the composite with 2.5 wt % *f*-MWCNTs had a grafting degree as low as 4−10%. These results clearly suggest that efficient exfoliation through covalent bonding following Scheme 1 is obtained for the composite with the lowest filler concentration. Increased filler concentrations eventually eliminate the proposed debundling action of the synthesis route. These

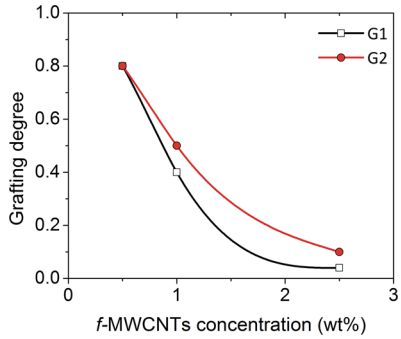

Figure 6. Grafting degree indices calculated from peak intensity (G1) and peak area (G2) ratios of N−C═O/C−N bonds.

results are consistent with the microscopy dispersion and bonding observations and with the viscosity and gyration radius calculations.

3.4. Structural Features of PCL/*f*-MWCNT Nanocomposites. The collected WAXD patterns of all the prepared materials are presented in Supporting Information Figure S4, revealing the characteristic PCL peaks at 21.4, 21.9, and 23.5° respectively. The calculated degree of crystallinity of PCL was 75.5%, whereas the nanocomposites with 0.5−1 wt % *f*-MWCNTs also presented increased crystallinities. Specifically, the nanocomposite containing 0.5 wt % *f*-MWCNTs had a crystallinity of 79.2%, whereas one containing 1 wt % *f*-MWCNTs had 78.7%. The composite with the highest filler loading had a slightly lower crystallinity compared to the other nanocomposites and the neat polymer sample, with a value of 74.2%. The calculated crystal size presented a similar trend. The neat polymer had a crystal size of 21.8 nm, whereas the composites with 0.5−1 wt % *f*-MWCNTs shared the same value of 23 nm. For the composite with 2.5 wt % *f*-MWCNTs, the crystal size was found to be almost the same as the neat polymer, namely, 21.9 nm. These values are within the range reported in literature for PCL materials.[72]

The higher crystalline content found in the nanocomposites with low filler amounts and their larger crystal size supports the previously discussed filler-exfoliation effect detected in these composites; therefore, mechanical property reinforcement efficiency is to be expected.[62,64,83] However in the highest filler loading, the crystal size similar to that of neat polymer and the lower degree of crystallinity compliment the insufficient filler exfoliation and its lower viscosity, implying that the improvement of the mechanical properties will not be adequate.

3.5. Mechanical Properties of PCL/*f*-MWCNT Nanocomposites. The mechanical properties of the PCL nano-

DOI: 10.1021/acsami.5b03693
ACS Appl. Mater. Interfaces 2015, 7, 11683−11694

Table 4. Mechanical Properties of PCL/*f*-MWCNT Nanocomposites

sample	E (MPa)	σ_y (MPa)	σ_b (MPa)	ε (%)	toughness (kJ/m^3)	impact strength (J/m)
PCL	290 ± 49	10.6 ± 1.5	13.1 ± 2.7	448 ± 47	37160 ± 11347	77.2 ± 0.1
PCL/0.5 wt % *f*-MWCNTs	326 ± 10	11.4 ± 0.6	20.0 ± 1.6	505 ± 54	59623 ± 9868	499.0 ± 1.9
PCL/1 wt % *f*-MWCNTs	489 ± 23	23.5 ± 5.1	20.3 ± 5.9	466 ± 75	63378 ± 23514	237.7 ± 4.8
PCL/2.5 wt % *f*-MWCNTs	251 ± 26	10.6 ± 1.6	6.8 ± 0.8	182 ± 47	12805 ± 2863	40.1 ± 0.1

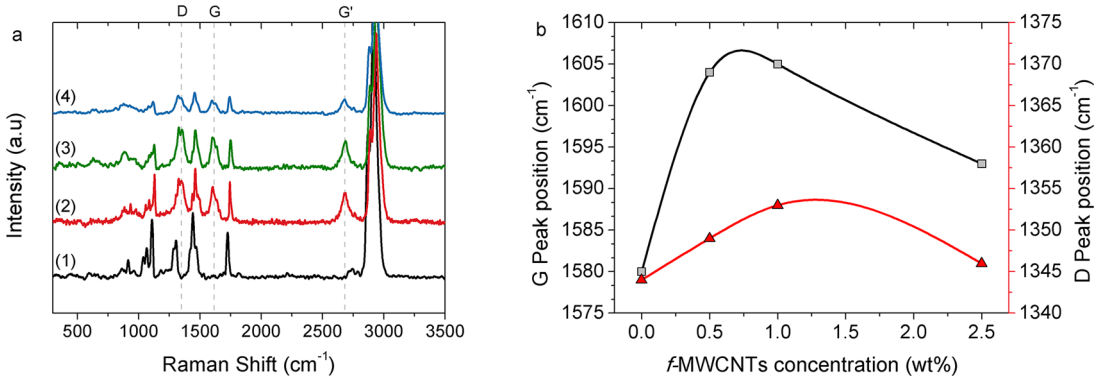

Figure 7. (a) Raman spectra and (b) the corresponding G and D peak shifts of all the prepared materials: (1) PCL, (2) PCL/0.5 wt % *f*-MWCNTs, (3) PCL/1 wt % *f*-MWCNTs, and (4) PCL/2.5 wt % *f*-MWCNTs.

composites were studied by tensile and impact testing. In general, the mechanical properties of polymer nanocomposites are strongly dependent on the good adhesion between the inorganic filler and the matrix and the dispersion of the filler as well as the crystalline characteristics of the material.[62,84] If dispersion and adhesion are adequate and the fillers interact with the matrix, then the applied load can be transferred effectively from the matrix to the nanofiller, and the mechanical properties are effectively enhanced. This effect is more likely to be achieved at low filler concentrations.[85−89] However, the tendency of the inorganic fillers to aggregate and form bundles, especially at higher contents, causes them to act as defects and stress concentrators in the matrix, which eventually prevents an effective reinforcement of the physical properties of the matrix. The results from the mechanical testing of PCL/*f*-MWCNT nanocomposites are presented in Table 4.

For the nanocomposites containing 0.5 wt % *f*-MWCNTs, the elastic modulus and yield strength were slightly improved compared to those of neat PCL. However, the incorporation of 1 wt % *f*-MWCNTs resulted in a significant stiffness enhancement. Specifically, the elastic modulus (E) enhancement exceeded 68% and the yield strength (σ_y) reinforcement 120%. However, for the 2.5 wt % *f*-MWCNTs composite, the elastic modulus was found to be lower than that of neat PCL, and the yield strength remained unaffected. The tensile strength at break (σ_b) was found to be significantly higher for both of 0.5 and 1 wt % *f*-MWCNTs composites (more than 50% increase in both cases), which is much higher than the corresponding increase (28%) mentioned by Kumar et al.[60] when amine-functionalized MWCNTs were added into PCL by melt mixing. A similar increase in the mechanical properties was also mentioned when MWCNTs functionalized with hydroxyl groups reacted by in situ ring-opening polymerization of LA and ε-CL monomers to covalently graft biodegradable PCLA copolymers onto MWCNTs surfaces.[69] The composite with the highest filler loading, however, exhibited significantly lower values, even lower than those of neat PCL.

The elongation at break presents a similar trend and was marginally higher than that of neat PCL in the 0.5 and 1 wt % *f*-MWCNTs composites, whereas a notable reduction was found for the highest filler concentration (2.5 wt %). The calculated toughness of 0.5 and 1 wt % *f*-MWCNTs composites was clearly higher than that of neat PCL (more than 60 and 70% respectively), indicating the exceptional performance of the specific samples. The most significant improvement was detected in the impact strength of the prepared nanocomposites. Particularly in the 0.5 wt % *f*-MWCNTs composite, the impact strength was more than 540% higher than that of neat PCL. A 200% higher impact strength was found for the PCL/1 wt % *f*-MWCNTs composite. However, as with most of its mechanical properties, both the toughness and impact strength of the 2.5 wt % *f*-MWCNTs composite were lower than the relative properties for the neat PCL.

The measured significant improvement of stiffness, ultimate strength, and impact performance of the composites with 0.5−1 wt % *f*-MWCNTs can be attributed to efficient filler exfoliation and the high degree of covalent grafting of the nanotubes and the polymer backbone, which lead to efficient filler exfoliation and ultimately improved dispersion. The formed interfaces, as evidenced through the covalent-bonding zones of the polymer-coated nanotubes (Figures 3 and 4), allow efficient load transfer from the matrix to the stiffer nanotubes, which combined with the enhanced crystallinity of the materials ultimately improves the mechanical properties of the composites.

Thus from the mechanical properties measurements, it was revealed that the incorporation of *f*-MWCNTs in PCL at concentrations lower than 1 wt % leads to a notable reinforcement because the nanotubes remain finely dispersed and covalently bonded to PCL macromolecules and can support the successful load transfer from the matrix. Moreover, on the basis of the higher stiffness and comparable deformation extent before fracture, the composites with 0.5−1 wt % *f*-MWCNTs have clearly retained the ductile fracture mode of PCL. However, increasing filler concentration yields a brittle performance, which can be associated with the large bundles of nanotubes formed during the composites preparation and the low amount of grafting to the polymer backbone. The nanotubes in an aggregated state cannot support load transfer

DOI: 10.1021/acsami.5b03693
ACS Appl. Mater. Interfaces 2015, 7, 11683−11694

and have lower adhesion with the matrix, resulting in inferior mechanical performance. Therefore, the positive effects of the incorporation of *f*-MWCNTs in PCL and its successful grafting to the macromolecular chains compete with the intrinsic van der Waals interactions that result in nanotube bundling and tend to reduce the properties reinforcement in the higher-filler-content materials. At low filler concentrations, the reinforcing mechanism rules over intrinsic forces, and a successful reinforcement is observed. In contrast, at the highest filler concentration, the intrinsic forces govern *f*-MWCNT incorporation in PCL, yielding inferior mechanical performance.

3.6. Load Transfer in PCL/*f*-MWCNT Nanocomposites. Raman spectroscopy has been extensively used in the literature in order to evaluate the interactions and provide estimations for the load transfer between polymeric matrixes and carbon-related fillers such as MWCNTs, which eventually are the main factors governing the physical properties and performance of the nanocomposite samples.[6490−92] MWCNTs present three characteristic bands in their Raman spectrum. A band at 1580 cm^{-1} (G band), which corresponds to the in-plane vibration of the C−C bonds and a shoulder around 1604 cm^{-1}, is typical for graphite-like materials with defects. The presence of the band at 1344 cm^{-1} (D band) indicates a certain level of disorder in the carbonaceous filler, whereas the band at around 2683 cm^{-1} is called the G′ band, attributed to the overtone of the D band.[93]

The results from the micro-Raman measurements on the PCL/*f*-MWCNT nanocomposites are presented in Figure 7. The characteristic bands of MWCNTs can be observed in all the nanocomposites, even for the lowest-filler-concentration nanocomposite. The G and D band positions observed in all the samples are presented in Figure 7b. It can be seen that for the nanocomposites with low filler content (0.5 and 1 wt %) shifts around 10 and 25 cm^{-1} for the D and G bands, respectively, were obtained. These notable shifts indicate the efficient exfoliation and successful load transfer from the matrix to the *f*-MWCNTs,[73,74,94−96] which is in agreement with all the previous findings. However, the sample with 2.5 wt % *f*-MWCNTs presents a smaller shift of the G and D bands, indicating a less efficient load transfer for that concentration. Therefore, the lower load transfer ability of the filler, which is associated with its highly bundled state, can clearly justify the reduced reinforcement efficiency of the filler in that concentration. This finding is in agreement with the reported significant mechanical properties enhancement with the low filler concentrations and the inferior performance found for the highest filler content.

4. CONCLUSIONS

In this work, amino-functionalized MWCNTs were incorporated into PCL via ring-opening polymerization, and the effects on the structure and mechanical properties of the materials were thoroughly investigated. It was found that *f*-MWCNTs allow polymerization to begin at considerably lower temperatures by reducing the required effective activation energy, and they also accelerate the reaction in all prepared concentrations. In the prepared nanocomposites, two competing mechanisms govern the *f*-MWCNTs incorporation in the matrix: a reinforcing trend because of successful covalent grafting, exfoliation, and dispersion of the filler and an aggregation trend that reduces the positive influence of the filler. At low concentrations, the reinforcing mechanism rules over intrinsic nanotube forces and a successful reinforcement is allowed. As nanotube content increases, the intrinsic bundling forces govern the MWCNTs incorporation in PCL, resulting in inferior mechanical performance for the highest concentration. In that case, the bonding between MWCNTs and the matrix as well as load transfer were low, yielding a poorer dispersion and therefore mediocre performance.

■ ASSOCIATED CONTENT

Ⓢ Supporting Information

XPS wide scans for all the prepared materials, high resolution spectra of *f*-MWCNTs and C 1s peaks deconvolution, and WAXD patterns of all the prepared materials. The Supporting Information is available free of charge on the ACS Publications website at DOI: 10.1021/acsami.5b03693.

■ AUTHOR INFORMATION

Corresponding Authors

*E-mail: eroumeli@auth.gr.

*E-mail: dbic@chem.auth.gr.

Notes

The authors declare no competing financial interest.

■ ACKNOWLEDGMENTS

We thank GLONATECH S.A for their kind allowance of *f*-MWCNTs. A.A. would like to acknowledge the Electron Microscopy Facility of the University of Ioannina for performing the necessary studies.

■ REFERENCES

(1) Paul, D. R.; Robeson, L. M. Polymer nanotechnology: Nanocomposites. *Polymer* **2008**, *49*, 3187−3204.

(2) Alexandre, M.; Dubois, P. Polymer-layered silicate nanocomposites: Preparation, properties and uses of a new class of materials. *Mater. Sci. Eng., R* **2000**, *28*, 1−63.

(3) Giannelis, E. P. Polymer-layered silicate nanocomposites: Synthesis, properties and applications. *Appl. Organomet. Chem.* **1998**, *12*, 675−680.

(4) Tjong, S. Structural and mechanical properties of polymer nanocomposites. *Mater. Sci. Eng., R* **2006**, *53*, 73−197.

(5) Alexandre, M.; Dubois, P. Polymer-layered silicate nanocomposites: preparation, properties and uses of a new class of materials. *Mater. Sci. Eng., R* **2000**, *28*, 1−63.

(6) Ikada, Y.; Tsuji, H. Biodegradable polyesters for medical and ecological applications. *Macromol. Rapid Commun.* **2000**, *21*, 117−132.

(7) Amass, W.; Amass, A.; Tighe, B. A review of biodegradable polymers: uses, current developments in the synthesis and characterization of biodegradable polyesters, blends of biodegradable polymers and recent advances in biodegradation studies. *Polym. Int.* **1998**, *47*, 89−144.

(8) Yoshimoto, H.; Shin, Y. M.; Terai, H.; Vacanti, J. P. A biodegradable nanofiber scaffold by electrospinning and its potential for bone tissue engineering. *Biomaterials* **2003**, *24*, 2077−2082.

(9) Lee, K.; Kim, H.; Khil, M.; Ra, Y.; Lee, D. Characterization of nano-structured poly (ε-caprolactone) nonwoven mats via electrospinning. *Polymer* **2003**, *44*, 1287−1294.

(10) Hiljanen-Vainio, M.; Karjalainen, T.; Seppälä, J. Biodegradable lactone copolymers. I. Characterization and mechanical behavior of ε-caprolactone and lactide copolymers. *J. Appl. Polym. Sci.* **1996**, *59*, 1281−1288.

(11) Sinha, V.; Bansal, K.; Kaushik, R.; Kumria, R.; Trehan, A. Poly-∈-caprolactone microspheres and nanospheres: an overview. *Int. J. Pharm.* **2004**, *278*, 1−23.

(12) Messersmith, P. B.; Giannelis, E. P. Synthesis and barrier properties of poly (ε-caprolactone)-layered silicate nanocomposites. *J. Polym. Sci., Part A: Polym. Chem.* **1995**, *33*, 1047−1057.

(13) Causa, F.; Netti, P.; Ambrosio, L.; Ciapetti, G.; Baldini, N.; Pagani, S.; Martini, D.; Giunti, A. Poly-∈-caprolactone/hydroxyapatite

DOI: 10.1021/acsami.5b03693
ACS Appl. Mater. Interfaces 2015, 7, 11683−11694

composites for bone regeneration: In vitro characterization and human osteoblast response. *J. Biomed. Mater. Res., Part A* **2006**, *76*, 151−162.
(14) Chrissafis, K.; Antoniadis, G.; Paraskevopoulos, K.; Vassiliou, A.; Bikiaris, D. Comparative study of the effect of different nanoparticles on the mechanical properties and thermal degradation mechanism of in situ prepared poly (ε-caprolactone) nanocomposites. *Compos. Sci. Technol.* **2007**, *67*, 2165−2174.
(15) Lepoittevin, B.; Pantoustier, N.; Devalckenaere, M.; Alexandre, M.; Kubies, D.; Calberg, C.; Jérôme, R.; Dubois, P. Poly (ε-caprolactone)/clay nanocomposites by in-situ intercalative polymerization catalyzed by dibutyltin dimethoxide. *Macromolecules* **2002**, *35*, 8385−8390.
(16) Chen, B.; Evans, J. R. Poly (ε-caprolactone)-clay nanocomposites: structure and mechanical properties. *Macromolecules* **2006**, *39*, 747−754.
(17) Kiersnowski, A.; Pigłowski, J. Polymer-layered silicate nanocomposites based on poly (ε-caprolactone). *Eur. Polym. J.* **2004**, *40*, 1199−1207.
(18) Viville, P.; Lazzaroni, R.; Pollet, E.; Alexandre, M.; Dubois, P.; Borcia, G.; Pireaux, J.-J. Surface characterization of poly (ε-caprolactone)-based nanocomposites. *Langmuir* **2003**, *19*, 9425−9433.
(19) Vassiliou, A. A.; Papageorgiou, G. Z.; Achilias, D. S.; Bikiaris, D. N. Non-Isothermal Crystallisation Kinetics of In Situ Prepared Poly (ε-caprolactone)/Surface-Treated SiO2 Nanocomposites. *Macromol. Chem. Phys.* **2007**, *208*, 364−376.
(20) Ajayan, P. M.; Stephan, O.; Colliex, C.; Trauth, D. Aligned carbon nanotube arrays formed by cutting a polymer resin-nanotube composite. *Science* **1994**, *265*, 1212−1214.
(21) Moniruzzaman, M.; Winey, K. I. Polymer Nanocomposites Containing Carbon Nanotubes. *Macromolecules* **2006**, *39*, 5194−5205.
(22) Du, F.; Scogna, R. C.; Zhou, W.; Brand, S.; Fischer, J. E.; Winey, K. I. Nanotube networks in polymer nanocomposites: rheology and electrical conductivity. *Macromolecules* **2004**, *37*, 9048−9055.
(23) Spitalsky, Z.; Tasis, D.; Papagelis, K.; Galiotis, C. Carbon nanotube−polymer composites: Chemistry, processing, mechanical and electrical properties. *Prog. Polym. Sci.* **2010**, *35*, 357−401.
(24) Hou, Y.; Tang, J.; Zhang, H.; Qian, C.; Feng, Y.; Liu, J. Functionalized Few-Walled Carbon Nanotubes for Mechanical Reinforcement of Polymeric Composites. *ACS Nano* **2009**, *3*, 1057−1062.
(25) Byrne, M. T.; Gun'ko, Y. K. Recent Advances in Research on Carbon Nanotube−Polymer Composites. *Adv. Mater. (Weinheim, Ger.)* **2010**, *22*, 1672−1688.
(26) Laird, E. D.; Li, C. Y. Structure and morphology control in crystalline polymer−carbon nanotube nanocomposites. *Macromolecules* **2013**, *46*, 2877−2891.
(27) Loos, M. R.; Manas-Zloczower, I. Reinforcement Efficiency of Carbon Nanotubes − Myth and Reality. *Macromol. Theory Simul.* **2012**, *21*, 130−137.
(28) Lu, W.; Zu, M.; Byun, J.-H.; Kim, B.-S.; Chou, T.-W. State of the Art of Carbon Nanotube Fibers: Opportunities and Challenges. *Adv. Mater. (Weinheim, Ger.)* **2012**, *24*, 1805−1833.
(29) Sakellariou, G.; Priftis, D.; Baskaran, D. Surface-initiated polymerization from carbon nanotubes: strategies and perspectives. *Chem. Soc. Rev.* **2013**, *42*, 677−704.
(30) Grossiord, N.; Loos, J.; Regev, O.; Koning, C. E. Toolbox for Dispersing Carbon Nanotubes into Polymers To Get Conductive Nanocomposites. *Chem. Mater.* **2006**, *18*, 1089−1099.
(31) Lin, P.; Cong, Y.; Zhang, B. Dispersing Carbon Nanotubes by Chiral Network Surfactants. *ACS Appl. Mater. Interfaces* **2015**, *7*, 6724−6732.
(32) Liu, Y.; Kumar, S. Polymer/Carbon Nanotube Nano Composite Fibers−A Review. *ACS Appl. Mater. Interfaces* **2014**, *6*, 6069−6087.
(33) Viswanathan, G.; Chakrapani, N.; Yang, H.; Wei, B.; Chung, H.; Cho, K.; Ryu, C. Y.; Ajayan, P. M. Single-Step in Situ Synthesis of Polymer-Grafted Single-Wall Nanotube Composites. *J. Am. Chem. Soc.* **2003**, *125*, 9258−9259.
(34) Lee, G.-W.; Jagannathan, S.; Chae, H. G.; Minus, M. L.; Kumar, S. Carbon nanotube dispersion and exfoliation in polypropylene and structure and properties of the resulting composites. *Polymer* **2008**, *49*, 1831−1840.
(35) Li, L.; Li, C. Y.; Ni, C. Polymer Crystallization-Driven, Periodic Patterning on Carbon Nanotubes. *J. Am. Chem. Soc.* **2006**, *128*, 1692−1699.
(36) Coleman, J. N.; Khan, U.; Gun'ko, Y. K. Mechanical Reinforcement of Polymers Using Carbon Nanotubes. *Adv. Mater. (Weinheim, Ger.)* **2006**, *18*, 689−706.
(37) Regev, O.; ElKati, P. N. B.; Loos, J.; Koning, C. E. Preparation of Conductive Nanotube−Polymer Composites Using Latex Technology. *Adv. Mater. (Weinheim, Ger.)* **2004**, *16*, 248−251.
(38) Xiao, Y.; Gong, T.; Zhou, S. The functionalization of multi-walled carbon nanotubes by in situ deposition of hydroxyapatite. *Biomaterials* **2010**, *31*, 5182−5190.
(39) Kubies, D.; Pantoustier, N.; Dubois, P.; Rulmont, A.; Jérôme, R. Controlled Ring-Opening Polymerization of ε-Caprolactone in the Presence of Layered Silicates and Formation of Nanocomposites. *Macromolecules* **2002**, *35*, 3318−3320.
(40) Liao, L.; Zhang, C.; Gong, S. Preparation of Poly(ε-caprolactone)/Clay Nanocomposites by Microwave-Assisted In Situ Ring-Opening Polymerization. *Macromol. Rapid Commun.* **2007**, *28*, 1148−1154.
(41) Saeed, K.; Park, S. Y. Preparation and properties of multiwalled carbon nanotube/polycaprolactone nanocomposites. *J. Appl. Polym. Sci.* **2007**, *104*, 1957−1963.
(42) Kim, H. S.; Park, B. H.; Yoon, J. S.; Jin, H. J. Preparation and characterization of multiwalled carbon nanotube/poly (ε-caprolactone) composites via in situ polymerization. *Solid State Phenom.* **2007**, *124*, 1133−1136.
(43) Mitchell, C. A.; Krishnamoorti, R. Non-isothermal crystallization of in situ polymerized poly(ε-caprolactone) functionalized-SWNT nanocomposites. *Polymer* **2005**, *46*, 8796−8804.
(44) Mitchell, C. A.; Krishnamoorti, R. Dispersion of Single-Walled Carbon Nanotubes in Poly(ε-caprolactone). *Macromolecules* **2007**, *40*, 1538−1545.
(45) Chin, S. J.; Vempati, S.; Dawson, P.; Knite, M.; Linarts, A.; Ozols, K.; McNally, T. Electrical conduction and rheological behaviour of composites of poly(ε-caprolactone) and MWCNTs. *Polymer* **2015**, *58*, 209−221.
(46) Villmow, T.; Kretzschmar, B.; Potschke, P. Influence of screw configuration, residence time, and specific mechanical energy in twin-screw extrusion of polycaprolactone/multi-walled carbon nanotube composites. *Compos. Sci. Technol.* **2010**, *70*, 2045−2055.
(47) Bello, A.; Laredo, E.; Marval, J. R.; Grimau, M.; Arnal, M. L.; Müller, A. J.; Ruelle, B.; Dubois, P. Universality and Percolation in Biodegradable Poly(ε-caprolactone)/Multiwalled Carbon Nanotube Nanocomposites from Broad Band Alternating and Direct Current Conductivity at Various Temperatures. *Macromolecules* **2011**, *44*, 2819−2828.
(48) Buffa, F.; Hu, H.; Resasco, D. E. Side-Wall Functionalization of Single-Walled Carbon Nanotubes with 4-Hydroxymethylaniline Followed by Polymerization of ε-Caprolactone. *Macromolecules* **2005**, *38*, 8258−8263.
(49) Meenarathi, B.; Chen, H.-H.; Chen, P.-H.; Anbarasan, R. Near infrared dye functionalized MWCNT as an effective initiator for the ring opening polymerization of ε-caprolactone. *J. Polym. Res.* **2013**, *20*, 1−12.
(50) Castro, M.; Lu, J.; Bruzaud, S.; Kumar, B.; Feller, J.-F. Carbon nanotubes/poly(ε-caprolactone) composite vapour sensors. *Carbon* **2009**, *47*, 1930−1942.
(51) Zeng, H. L.; Gao, C.; Yan, D. Y. Poly(ε-caprolactone)-Functionalized Carbon Nanotubes and Their Biodegradation Properties. *Adv. Funct. Mater.* **2006**, *16*, 812−818.
(52) Pérez, R. A.; López, J. V.; Hoskins, J. N.; Zhang, B.; Grayson, S. M.; Casas, M. T.; Puiggalí, J.; Müller, A. J. Nucleation and Antinucleation Effects of Functionalized Carbon Nanotubes on Cyclic and Linear Poly(ε-caprolactones). *Macromolecules* **2014**, *47*, 3553−3566.

DOI: 10.1021/acsami.5b03693
ACS Appl. Mater. Interfaces 2015, 7, 11683−11694

(53) Priftis, D.; Sakellariou, G.; Hadjichristidis, N.; Penott, E. K.; Lorenzo, A. T.; Müller, A. J. Surface modification of multiwalled carbon nanotubes with biocompatible polymers via ring opening and living anionic surface initiated polymerization. Kinetics and crystallization behavior. *J. Polym. Sci., Part A: Polym. Chem.* **2009**, *47*, 4379−4390.
(54) Ruelle, B.; Peeterbroeck, S.; Gouttebaron, R.; Godfroid, T.; Monteverde, F.; Dauchot, J.-P.; Alexandre, M.; Hecq, M.; Dubois, P. Functionalization of carbon nanotubes by atomic nitrogen formed in a microwave plasma Ar + N_2 and subsequent poly([varepsilon]-caprolactone) grafting. *J. Mater. Chem.* **2007**, *17*, 157−159.
(55) Dubois, P.; Degee, P.; Jerome, R.; Teyssie, P. Macromolecular engineering of polylactones and polylactides. 8. Ring-opening polymerization of ϵ-caprolactone initiated by primary amines and trialkylaluminum. *Macromolecules* **1992**, *25*, 2614−2618.
(56) Zhou, B.; Tong, Z.-Z.; Huang, J.; Xu, J.-T.; Fan, Z.-Q. Synthesis and thermal behavior of poly(ε-caprolactone) grafted on multiwalled carbon nanotubes with high grafting degrees. *Mater. Chem. Phys.* **2013**, *137*, 1053−1061.
(57) Lee, R.-S.; Chen, W.-H.; Lin, J.-H. Polymer-grafted multi-walled carbon nanotubes through surface-initiated ring-opening polymerization and click reaction. *Polymer* **2011**, *52*, 2180−2188.
(58) Yang, Y.; Tsui, C. P.; Tang, C. Y.; Qiu, S.; Zhao, Q.; Cheng, X.; Sun, Z.; Li, R. K. Y.; Xie, X. Functionalization of carbon nanotubes with biodegradable supramolecular polypseudorotaxanes from grafted-poly(ε-caprolactone) and α-cyclodextrins. *Eur. Polym. J.* **2010**, *46*, 145−155.
(59) Zhou, B.; He, W.-N.; Jiang, X.-Y.; Tong, Z.-Z.; Xu, J.-T.; Fan, Z.-Q. Effect of molecular weight on isothermal crystallization kinetics of multi-walled carbon nanotubes-graft-poly(ε-caprolactone). *Compos. Sci. Technol.* **2014**, *93*, 23−29.
(60) Kumar, S.; Bose, S.; Chatterjee, K. Amine-functionalized multiwall carbon nanotubes impart osteoinductive and bactericidal properties in poly([varepsilon]-caprolactone) composites. *RSC Adv.* **2014**, *4*, 19086−19098.
(61) Limwanich, W.; Meepowpan, P.; Nalampang, K.; Kungwan, N.; Molloy, R.; Punyodom, W. Kinetics and thermodynamics analysis for ring-opening polymerization of ε-caprolactone initiated by tributyltin n-butoxide using differential scanning calorimetry. *J. Therm. Anal. Calorim.* **2014**, *119*, 567−579.
(62) Roumeli, E.; Pavlidou, E.; Avgeropoulos, A.; Vourlias, G.; Bikiaris, D. N.; Chrissafis, K. Factors controlling the enhanced mechanical and thermal properties of nanodiamond-reinforced cross-linked high density polyethylene. *J. Phys. Chem. B* **2014**, *118*, 11341−11352.
(63) Papageorgiou, G. Z.; Papageorgiou, D. G.; Tsanaktsis, V.; Bikiaris, D. N. Synthesis of the bio-based polyester poly(propylene 2,5-furan dicarboxylate). Comparison of thermal behavior and solid state structure with its terephthalate and naphthalate homologues. *Polymer* **2015**, *62*, 28−38.
(64) Roumeli, E.; Avgeropoulos, A.; Pavlidou, E.; Vourlias, G.; Kyratsi, T.; Bikiaris, D.; Chrissafis, K. Understanding the mechanical and thermal property reinforcement of crosslinked polyethylene by nanodiamonds and carbon nanotubes. *RSC Adv.* **2014**, *4*, 45522−45534.
(65) Ebewele, R. O. *Polymer Science and Technology*; CRC Press: Taylor & Francis, 2000.
(66) Starink, M. J. The determination of activation energy from linear heating rate experiments: a comparison of the accuracy of isoconversion methods. *Thermochim. Acta* **2003**, *404*, 163−176.
(67) Vyazovkin, S. Kinetic concepts of thermally stimulated reactions in solids: A view from a historical perspective. *Int. Rev. Phys. Chem.* **2000**, *19*, 45−60.
(68) Jana, R. N.; Cho, J. W. Thermal stability, crystallization behavior, and phase morphology of poly(ϵ-caprolactone)diol-grafted-multiwalled carbon nanotubes. *J. Appl. Polym. Sci.* **2008**, *110*, 1550−1558.
(69) Chakoli, A. N.; Wan, J.; Feng, J. T.; Amirian, M.; Sui, J. H.; Cai, W. Functionalization of multiwalled carbon nanotubes for reinforcing of poly(L-lactide-co-ε-caprolactone) biodegradable copolymers. *Appl. Surf. Sci.* **2009**, *256*, 170−177.
(70) Müller, A. J.; Arnal, M. L.; Trujillo, M.; Lorenzo, A. T. Super-nucleation in nanocomposites and confinement effects on the crystallizable components within block copolymers, miktoarm star copolymers and nanocomposites. *Eur. Polym. J.* **2011**, *47*, 614−629.
(71) Ding, W.; Eitan, A.; Fisher, F. T.; Chen, X.; Dikin, D. A.; Andrews, R.; Brinson, L. C.; Schadler, L. S.; Ruoff, R. S. Direct Observation of Polymer Sheathing in Carbon Nanotube−Polycarbonate Composites. *Nano Lett.* **2003**, *3*, 1593−1597.
(72) Castilla-Cortázar, I.; Más-Estellés, J.; Meseguer-Dueñas, J. M.; Escobar Ivirico, J. L.; Marí, B.; Vidaurre, A. Hydrolytic and enzymatic degradation of a poly(ε-caprolactone) network. *Polym. Degrad. Stab.* **2012**, *97*, 1241−1248.
(73) Enotiadis, A.; Litina, K.; Gournis, D.; Rangou, S.; Avgeropoulos, A.; Xidas, P.; Triantafyllidis, K. Nanocomposites of Polystyrene-*b*-Poly(isoprene)-*b*-Polystyrene Triblock Copolymer with Clay−Carbon Nanotube Hybrid Nanoadditives. *J. Phys. Chem. B* **2013**, *117*, 907−915.
(74) Litina, K.; Miriouni, A.; Gournis, D.; Karakassides, M. A.; Georgiou, N.; Klontzas, E.; Ntoukas, E.; Avgeropoulos, A. Nanocomposites of polystyrene-b-polyisoprene copolymer with layered silicates and carbon nanotubes. *Eur. Polym. J.* **2006**, *42*, 2098−2107.
(75) Kalathi, J. T.; Grest, G. S.; Kumar, S. K. Universal Viscosity Behavior of Polymer Nanocomposites. *Phys. Rev. Lett.* **2012**, *109*, 198301.
(76) Zhang, Q.; Lippits, D. R.; Rastogi, S. Dispersion and Rheological Aspects of SWNTs in Ultrahigh Molecular Weight Polyethylene. *Macromolecules* **2006**, *39*, 658−666.
(77) Grady, B. P. The Use of Solution Viscosity to Characterize Single-Walled Carbon Nanotube Dispersions. *Macromol. Chem. Phys.* **2006**, *207*, 2167−2169.
(78) Cotiuga, I.; Picchioni, F.; Agarwal, U. S.; Wouters, D.; Loos, J.; Lemstra, P. J. Block-Copolymer-Assisted Solubilization of Carbon Nanotubes and Exfoliation Monitoring Through Viscosity. *Macromol. Rapid Commun.* **2006**, *27*, 1073−1078.
(79) Bikiaris, D.; Karavelidis, V.; Karayannidis, G. A New Approach to Prepare Poly(ethylene terephthalate)/Silica Nanocomposites with Increased Molecular Weight and Fully Adjustable Branching or Crosslinking by SSP. *Macromol. Rapid Commun.* **2006**, *27*, 1199−1205.
(80) Vasileiou, A. A.; Papageorgiou, G. Z.; Kontopoulou, M.; Docoslis, A.; Bikiaris, D. Covalently bonded poly(ethylene succinate)/SiO_2 nanocomposites prepared by *in situ* polymerisation. *Polymer* **2013**, *54*, 1018−1032.
(81) Vassiliou, A. A.; Bikiaris, D.; El Mabrouk, K.; Kontopoulou, M. Effect of evolved interactions in poly(butylene succinate)/fumed silica biodegradable in situ prepared nanocomposites on molecular weight, material properties, and biodegradability. *J. Appl. Polym. Sci.* **2011**, *119*, 2010−2024.
(82) Vassiliou, A. A.; Papageorgiou, G. Z.; Achilias, D. S.; Bikiaris, D. N. Non-Isothermal Crystallisation Kinetics of In Situ Prepared Poly(ε-caprolactone)/Surface-Treated SiO_2 Nanocomposites. *Macromol. Chem. Phys.* **2007**, *208*, 364−376.
(83) Kim, H.-S.; Chae, Y. S.; Choi, J. H.; Yoon, J.-S.; Jin, H.-J. Thermal Properties of Poly(ε-Caprolactone)/Multiwalled Carbon Nanotubes Composites. *Adv. Compos. Mater.* **2008**, *17*, 157−166.
(84) Papageorgiou, D. G.; Tzounis, L.; Papageorgiou, G. Z.; Bikiaris, D. N.; Chrissafis, K. β-nucleated propylene−ethylene random copolymer filled with multi-walled carbon nanotubes: Mechanical, thermal and rheological properties. *Polymer* **2014**, *55*, 3758−3769.
(85) Istrate, O. M.; Paton, K. R.; Khan, U.; O'Neill, A.; Bell, A. P.; Coleman, J. N. Reinforcement in melt-processed polymer−graphene composites at extremely low graphene loading level. *Carbon* **2014**, *78*, 243−249.
(86) Liang, J.; Huang, Y.; Zhang, L.; Wang, Y.; Ma, Y.; Guo, T.; Chen, Y. Molecular-Level Dispersion of Graphene into Poly(vinyl alcohol) and Effective Reinforcement of their Nanocomposites. *Adv. Funct. Mater.* **2009**, *19*, 2297−2302.

DOI: 10.1021/acsami.5b03693
ACS Appl. Mater. Interfaces 2015, 7, 11683−11694

(87) Shi, D.; Lian, J.; He, P.; Wang, L. M.; Xiao, F.; Yang, L.; Schulz, M. J.; Mast, D. B. Plasma coating of carbon nanofibers for enhanced dispersion and interfacial bonding in polymer composites. *Appl. Phys. Lett.* **2003**, *83*, 5301−5303.
(88) Paiva, M. C.; Zhou, B.; Fernando, K. A. S.; Lin, Y.; Kennedy, J. M.; Sun, Y. P. Mechanical and morphological characterization of polymer−carbon nanocomposites from functionalized carbon nanotubes. *Carbon* **2004**, *42*, 2849−2854.
(89) Papageorgiou, D. G.; Vourlias, G.; Bikiaris, D. N.; Chrissafis, K. Synergistic Effect of Functionalized Silica Nanoparticles and a β-Nucleating Agent for the Improvement of the Mechanical Properties of a Propylene/Ethylene Random Copolymer. *Macromol. Mater. Eng.* **2014**, *299*, 707−721.
(90) Roumeli, E.; Pavlidou, E.; Bikiaris, D.; Chrissafis, K. Microscopic observation and micromechanical modeling to predict the enhanced mechanical properties of multi-walled carbon nanotubes reinforced crosslinked high density polyethylene. *Carbon* **2014**, *67*, 475−487.
(91) Vallés, C.; Kinloch, I. A.; Young, R. J.; Wilson, N. R.; Rourke, J. P. Graphene oxide and base-washed graphene oxide as reinforcements in PMMA nanocomposites. *Compos. Sci. Technol.* **2013**, *88*, 158−164.
(92) Gong, L.; Young, R. J.; Kinloch, I. A.; Haigh, S. J.; Warner, J. H.; Hinks, J. A.; Xu, Z.; Li, L.; Ding, F.; Riaz, I.; Jalil, R.; Novoselov, K. S. Reversible Loss of Bernal Stacking during the Deformation of Few-Layer Graphene in Nanocomposites. *ACS Nano* **2013**, *7*, 7287−7294.
(93) Schadler, L. S.; Giannaris, S. C.; Ajayan, P. M. Load transfer in carbon nanotube epoxy composites. *Appl. Phys. Lett.* **1998**, *73*, 3842−3844.
(94) Minfang, M.; Sebastian, O.; Yury, G.; Karen, I. W. An in situ Raman spectroscopy study of stress transfer between carbon nanotubes and polymer. *Nanotechnology* **2009**, *20*, 335703.
(95) Rahmat, M.; Hubert, P. Carbon nanotube−polymer interactions in nanocomposites: A review. *Compos. Sci. Technol.* **2011**, *72*, 72−84.
(96) de la Vega, A.; Kinloch, I. A.; Young, R. J.; Bauhofer, W.; Schulte, K. Simultaneous global and local strain sensing in SWCNT−epoxy composites by Raman and impedance spectroscopy. *Compos. Sci. Technol.* **2011**, *71*, 160−166.

DOI: 10.1021/acsami.5b03693
ACS Appl. Mater. Interfaces 2015, 7, 11683−11694